JOURNAL OF THERMOPHYSICS AND HEAT TRANSFER
Vol. 23, No. 2, April–June 2009

Development of a Fire Zone Model Considering Mixing Behavior

Shaodong Guo,* Rui Yang,† and Hui Zhang‡
Tsinghua University, 100084 Beijing, People's Republic of China
and
Satish Narayanan§ and Mauro Atalla¶
United Technologies Research Center, East Hartford, Connecticut 06108

DOI: 10.2514/1.41240

A new zone model is proposed to compute smoke propagation and characterize smoke mixing behavior in complex enclosed spaces. A piecewise linear scalar function considering the mixing between the hot smoke and the cold air is introduced to better resolve the temperature and smoke profiles in the vertical direction. The mixing properties are approximated and characterized as turbulent transport of momentum and energy. The governing equations considering mixing effects are derived in terms of the scalar function. Two test cases are used to evaluate the model. First, the model predictions are compared with those from the two-layer model implemented using CFAST (Consolidated Model of Fire and Smoke Transport, developed by the National Institute of Standards and Technology) and experimental data reported in the literature for a simple setting involving an interconnected set of enclosed spaces. Second, the model prediction results are compared to that from a computational fluid dynamics model, namely, FLUENT, for a two-story office building. It is shown that the newly proposed model provides more accurate predictions of temperature distributions compared to that predicted by the two-layer model and is significantly less computationally expensive when compared to a computational fluid dynamics approach. Finally, the model presented provides a new framework for zone modeling using scalar functions, in which the traditional network model and the two-layer model can be reconstructed from different distribution functions.

Nomenclature

C = concentration, kg/kg
C_p = constant-pressure specific heat, $m^2 \cdot s^{-2} \cdot K^{-1}$
C_v = constant-volume specific heat, $m^2 \cdot s^{-2} \cdot K^{-1}$
D = diffusion coefficient, $m^2 \cdot s^{-1}$
F = scalar function
F_C = scalar function for the concentration
F_k = scalar function in the kth zone
F_T = scalar function for the temperature
H = height, m
H_{bot} = height of bottom of lower layer, m
H_{int} = height of the isoline for $F = 0.5$, m
$\bar{H}_L$ = equivalent enthalpy in upper layer, J
H_{top} = height of top of upper layer, m
$\bar{H}_U$ = equivalent enthalpy in upper layer, J
H_k^{cold} = height of top of cold layer in the kth zone, m
H_k^{hot} = height of bottom of hot layer in the kth zone, m
$\bar{M}_L$ = equivalent mass in lower layer, kg
$\bar{M}_U$ = equivalent mass in upper layer, kg
m_s^L = mass of the s specie being tracked in the lower layer, kg
m_s^U = mass of the s specie being tracked in the upper layer, kg
P = pressure, Pa
Pr_t = turbulent Prandtl number
R = gas constant, $J \cdot mol^{-1} \cdot K^{-1}$
R_T = turbulent Reynolds number
S = spreading rate
T = temperature, K
$\bar{T}_L$ = equivalent temperature in lower layer, K
$\bar{T}_U$ = equivalent temperature in upper layer, K
t = time, s
U_0 = characteristic velocity scale, $m\,s^{-1}$
V = volume, m^3
V_L = volume of lower layer, m^3
x = characteristic length, m
α = thermal expansion coefficient
α_e = effective thermal expansion coefficient
γ = specific heat ratio
$\overline{\Delta p}$ = pressure difference, Pa
$\overline{\Delta T}$ = average temperature rise, K
ν_e = effective viscosity, $m^2 \cdot s^{-1}$
ν_l = laminar viscosity, $m^2 \cdot s^{-1}$
ν_t = turbulent eddy viscosity, $m^2 \cdot s^{-1}$
ρ = density, $kg \cdot m^{-3}$
$\bar{\rho}_L$ = equivalent density in lower layer, $kg \cdot m^{-3}$
$\bar{\rho}_U$ = equivalent density in upper layer, $kg \cdot m^{-3}$
ϕ_L = physical properties in lower layer
$\bar{\phi}_L$ = equivalent physical properties in lower layer
ϕ_U = physical properties in upper layer
$\bar{\phi}_U$ = equivalent physical properties in upper layer

Received 26 September 2008; revision received 28 December 2008; accepted for publication 25 January 2009.

*Ph.D. Candidate, Department of Engineering Physics, and Department of Engineering Mechanics, School of Aerospace.
†Associate Professor, Department of Engineering Physics.
‡Professor, Department of Engineering Physics.
§Principle Engineer/Scientist, UTC Fire and Security Program Office, 411 Silver Lane.
¶Director, UTC Fire and Security Program Office, 411 Silver Lane.

I. Introduction

SMOKE inhalation is the leading cause of occupant fatalities in building fires. Several types of models have been developed to simulate smoke propagation during a building fire. These models have different degrees of simplification, from empirical ones with correlations based on dimensional analysis to semi-empirical ones (zone models [1–8]), and to physics-based models (field models [9–14] to field-zone models [15–20]) based on computational fluid dynamics (CFD). Among these, zone models have evolved from the use of observations in realistic fire experiments and need less

computational resources, enabling rapid computation and analysis. Thus, zone models are amenable to simulation of high-rise building fires and to optimize the detector and suppression configuration subject to multiple threat scenarios and building topologies.

According to a recent survey [21], 51 actively supported zone models are available. Most of these models use at most two control volumes to describe a compartment: an upper hot smoke layer and a lower cold air layer. These models assume that the predicted condition within each layer has uniform properties, namely, for temperature, smoke density, gas concentration, etc.

It is evident that as time progresses, the smoke and the cold air will mix rapidly within a small distance so that distinct layers are not discernible. The two-layer model is unable to accurately capture the mixing between the upper and the lower layers, and to simulate the smooth variation of temperature from the upper (hot) smoke layer to the lower (cold) air layer, which results in inaccurate predictions from the two-layer model, especially in a multiroom building with long corridors where smoke diffusion can be significant. Typically, temperature and smoke concentration in the upper layer are overpredicted, whereas temperature and smoke concentration in the lower layer are underestimated [8]. Since before flashover, the occupants are primarily exposed to the lower layer, it is crucial to consider the mixing between the hot and cold layers for determining the vitiation of the lower layer with combustion products. A possible remedy for this type of zone modeling, without significantly increasing computational expense, would be to improve the vertical resolution of the zone model using a three-layer model [20].

Charters et al. [22] developed a three-layer model (called FASIT) for tunnel fires, to characterize the mixing behavior of the two layers described previously. In this model, the computational domain is divided into different zones, with each zone having three layers and two interfaces. (Note that the terms zone and layer are used here to indicate horizontal and vertical "interfaces," respectively.) Constant properties, such as velocity, concentration, and temperature, are assigned for each layer. The weakness of this model is the requirement to track the dynamics of two interfaces. Tracking a moving interface is feasible for the tunnel fire problem because the boundary conditions are relatively simple. However, such a feature presents challenges for simulating fire in a building indoor environment with doors and windows which can be open or closed at any time. New correlations for the interactions of the multiple layers passing through windows/doors are needed.

Suzuki et al. [23] developed a multilayer model to predict vertical distributions of temperature for a single-room fire. In this model, the space in a compartment was divided into an arbitrary number of control volumes. The predictions showed good agreement with experiments. However, it would be difficult to extend such a model to a multiroom building, because many more layers will be needed, leading to more interfaces that must be tracked as the fire evolves, and there will be difficulty in determining the mass exchange between the vents and the layers.

In this paper, a new zone modeling approach is proposed and a model is developed to simulate the mixing and the transition between two layers. A scalar function is introduced to describe the mixing and used to determine the temporal and spatial distribution of the physical properties between the hot and cold layers. There are several zone models available for fire simulations and some of them can be considered as special cases of this model. In the proposed model, distinct from traditional three-layer [22] and multilayer models [23], physical conditions are not assumed to be uniform in the mixing layer. Numerical predictions using the newly proposed model are compared with the experimental results and those from simulations of Consolidated Model of Fire and Smoke Transport (CFAST) [8] (a two-layer zone model), and FLUENT [14] (a computational fluid dynamics–CFD-based field model) for fires in two different building structures. This paper reports early model development efforts and further improvements of the scalar function, validation, and refinement of the model are being necessary and being pursued. In particular, detailed efforts are underway to understand the sensitivity of the model to building geometry, boundary conditions, and fire scenarios.

II. Fundamentals of the Three-Layer Model

A. Flow Patterns

Zukoski et al. [24] and Lim et al. [25] conducted a series of experiments to study flow patterns, mixing behavior, and heat transfer of room fires. The schematics of a "three-layer" flow pattern were shown in their papers to explain and characterize the phenomenon observed in their experiments (Fig. 7 in [24] and Fig. 2.3 in [25]). From the figures, two interfaces were clearly observed, illustrating a three-layer pattern in a corridor. The top layer is filled with hot smoke due to the buoyant effect, while the bottom layer is a cooler air layer with little smoke vitiation. It is also evident from such experiments that the transition between the top and bottom layers is gradual rather than abrupt and sharp as assumed in two-layer models.

To characterize the three-layer pattern, we first describe its formation. Consider a building enclosure with a small room with an open door leading to a corridor [24]. When fire starts in the room, fresh air is entrained into the plume, and the smoke rises to form a layer of hot gas near the ceiling in the fire source room. As time progresses, the hot gas in the room begins to flow out of the door into the adjacent corridor. The gas forms a buoyant plume, impinges on the ceiling, and produces a thin jet along the ceiling, see Fig. 1d in [24]. A hot layer is thus formed. As the air continues to be entrained to the hot layer in the fire room and the hot gas continues to enter the corridor from the doorway, the hot layer in the corridor continues to grow. The flow behavior is similar to that of a mixing layer separating the hot and cold layers [25]. Thus, a three-layer pattern in the corridor emerges. (See Fig. 2.3 in [25] for a detailed description.)

In the next section, the equations to describe the three-layer pattern will be presented, some of which (such as the linear representation for the scalar function F) will be obtained from experimental data [25,26].

B. Physical Properties

In this model, the computational domain is divided into different zones. Following the description in Sec. II.A, hot, mixing, and cold layers are set up for each zone.

It is known that the mean profile of a turbulent mixing layer is self-similar [27,28]. The self-similarity has been evidenced and verified by direct numerical simulation [29] and several experiments [30]. A scalar function F is introduced to describe the smoke vertical profile so that physical properties such as smoke concentration, temperature, and flow velocity can be represented. In general, F is a function of height, and various environmental conditions, and changes with time. The physical properties ϕ are defined by F in $\phi = \phi(\phi_{\max}, \phi_{\min}, F)$, where $\phi_{\max}$ and $\phi_{\min}$ denote the maximum and minimum values of physical properties in the upper and lower layers.

The scalar function F increases from 0 to 1 from the floor to the ceiling, as shown in Fig. 1, which is a function of space (field variables) and time. If F takes only two values of zero and unity, it would revert to a traditional two-layer model. If F has three values, the conventional three-layer model (namely, FASIT [22]) is recovered. Generally, the equations for F must be established and solved with grids such as volume of fluid or level-set methods to obtain an accurate distribution. However, because there is no mesh in the zone model, an alternative method to obtain F must be explored.

Several experiments were conducted to investigate the temperature distribution. For example, Steckler et al. [26] conducted a series of full-scale fire experiments to measure the vertical temperature distribution using aspirated thermocouples. From the experiments, it was found that although the magnitudes of the temperatures are different due to different fire strengths, the distribution profiles are similar. Furthermore, the vertical distribution of temperature in the mixing layer was found to be almost linear (see Fig. 1). Thus, in the present model, a linear form for F, which changes linearly from zero to unity from the floor to the ceiling, is used. Each zone can then be divided into three layers: a hot, a mixing, and a cold layer. F can be assigned to be zero in the cold layer, be linear (namely, in the range zero to unity) for the mixing layer, and be unity in the hot layer, as

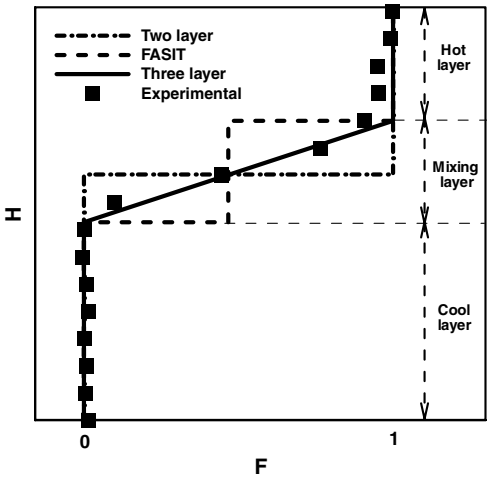

Fig. 1 The scalar F functions of the two-layer model, the FASIT model, and the three-layer model, with experimental data shown using symbols.

illustrated in Fig. 1. Thus, a new three-layer model can be derived in terms of the scalar function. Assuming self-similar-like behavior of the mixing layer [27,28], physical properties, such as the temperature of the layer gas and the wall segment, and mass of species, in this model can be described in terms of F, determined as follows:

$$\phi(F) = \phi_U F + \phi_L(1-F) \tag{1}$$

Lim et al. [25] conducted a series of experiments, where they measured both the temperature and carbon dioxide concentration at different times, and both profiles showed self-similarity (see Figs. 3.4–3.10 in [25]). In the current three-layer model, F is given as follows:

$$\begin{cases} F_k(t,H) = 0 & H \le H_k^{\text{cold}}(t) \\ F_k(t,H) = \frac{H - H_k^{\text{cold}}(t)}{H_k^{\text{hot}}(t) - H_k^{\text{cold}}(t)} & H_k^{\text{cold}}(t) < H < H_k^{\text{hot}}(t) \\ F_k(t,H) = 1 & H \ge H_k^{\text{hot}}(t) \end{cases} \tag{2}$$

where H_k^{hot} and H_k^{cold} are the height of the bottom of the hot layer and the top of the cold layer in the kth zone, respectively, determined by the location of isoline $F = 0.5$ and the thickness of the mixing layer.

With the current choice of F, a three-layer structure is constructed: an upper hot smoke layer, a lower cold air layer, and a mixing layer. In the upper and lower layers, the thermal physical properties F_U and F_L are uniform, while in the mixing layer, physical properties F increase linearly from F_L to F_U.

Other forms of the scalar function with some control parameters can be chosen to correct the linear assumption according to experimental observations. One such scalar function is the error function. For the mixing layer with constant turbulent viscosity, the self-similar profile is an error function [31],

$$F_C = 1 - \text{erf}\left(\frac{x}{2\sqrt{Dt}}\right) \qquad F_T = 1 - \text{erf}\left(\frac{x}{2\sqrt{\alpha t}}\right) \tag{3}$$

It is known that for a diffusion process from a higher concentration or temperature to a lower one that (see Fig. 2)

$$\frac{C_{\text{high}} - C}{C_{\text{high}} - C_{\text{low}}} = \text{erf}\left(\frac{x}{2\sqrt{Dt}}\right) \qquad \frac{T_{\text{high}} - T}{T_{\text{high}} - T_{\text{low}}} = \text{erf}\left(\frac{x}{2\sqrt{\alpha t}}\right)$$

where D (α) is the diffusion coefficient, t is the diffusion time, C (T) is the concentration (temperature) at a distance x from C_{high} (T_{high}), and erf is the error function defined as

$$\text{erf}(\eta) = \frac{2}{\sqrt{\pi}} \int_0^{\eta} \exp(-\eta^2) \mathrm{d}\eta$$

Thus, the mixing behavior between the upper hot smoke layer and the lower cold air layer can be characterized using the error function. And the scalar F can be determined in terms of the error function.

We plot both kinds of the F function in Fig. 2. Because in the current model, the temperature can be described in terms of F, and determined by the linear relation (1), the characteristic of temperature distribution should be similar to that of the F function. From Fig. 2, the difference is evident only in the smoothness of transitions from the top to the middle regimes and from the middle to the bottom regimes. Thus, for simplicity, although we have not simulated the temperature distribution using the error function, from the F function shown in Fig. 2, we presume that in most of the mixing layer, the temperature distribution predicted by these two functions should be similar.

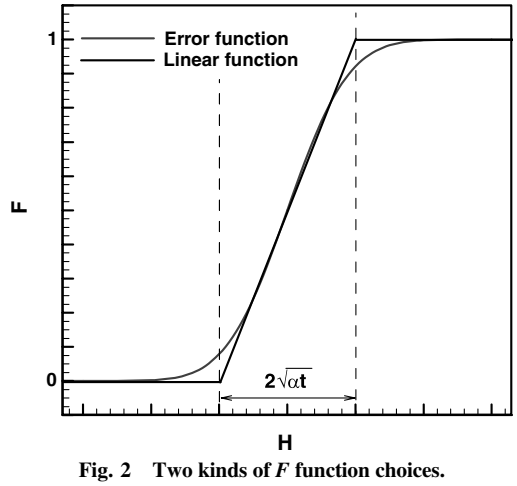

Fig. 2 Two kinds of F function choices.

C. Mixing Properties

As time progresses and with increasing distance, mixing will be strong and the middle layer will grow outward. Thus, mixing between the upper hot smoke layer and the lower cold air layer should be accounted for. This can be approximated and characterized as turbulent transport of momentum and energy. The thickness of thermal and flow boundary layers is dependent on the turbulent Prandtl number Pr_t, effective viscosity ν_e and diffusion time t as follows:

$$\begin{aligned} H^*_{\text{hot}} - H^*_{\text{cold}} &= 2\sqrt{\nu_e t} \qquad \nu_e = \nu_t + \nu_l \\ H^{**}_{\text{hot}} - H^{**}_{\text{cold}} &= 2\sqrt{\alpha_e t} \qquad \alpha_e = \frac{\nu_e}{P_{\text{rt}}} \end{aligned} \tag{4}$$

where superscript * denotes momentum diffusion and superscript ** denotes thermal diffusion. ν_t and ν_l are defined as the turbulent eddy viscosity and laminar viscosity, respectively. The effective viscosity ν_e, which must be obtained using a turbulence model in the CFD [32], is assumed to be a constant value in this model. Following the arguments presented in Sec. II.A, the flow behavior can be assumed to be close to that of a turbulent shear layer [27,28]. Thus, an ideal shear turbulent with uniform turbulent viscosity assumption, an algebraic turbulence model, was used to approximate the magnitude and scale of the turbulent viscosity. An analytical solution can then be obtained by solving the self-similar boundary-layer equation [27,28]:

$$\nu_t = \frac{U_0 l(x)}{R_T} = \frac{\sqrt{2\Delta p/\rho}}{R_T} Sx \tag{5}$$

where U_0 denotes the characteristic velocity scale, $U_0 \approx \sqrt{2\Delta p/\rho}$, and S and x denote the spreading rate and the characteristic length, respectively. Several experiments reveal an almost constant spreading rate S. For example, the spreading rate measured by Panchapakesan and Lumley [33] is 0.096 with $Re = 11,000$, and the spreading rate measured by Hussein et al. [34] is 0.102 with $Re = 95,500$. We therefore adopt the experimental value $S \approx 0.1$.

R_T denotes the turbulent Reynolds number which is a constant, $R_T \approx 31$ for the plane jet, and $R_T \approx 35$ for the round jet. Substituting into Eq. (5), an approximation to the turbulent viscosity can be obtained. Fang and Wu [35] measured the value of the turbulent Prandtl number (Pr_t) in a turbulent buoyant flow, which is about 0.8–1.0. Other experiments also indicated that Pr_t for air is about 1.0–1.6. So $Pr_t \approx 1$ is used in the current model. If Pr_t for air is taken to be unity, that is, the thermal and viscous diffusivity are assumed to be the same, the thicknesses of the thermal and flow boundary layers become the same. For the linear piecewise function F, the control parameters are $H_k^{\text{cold}}(t)$ and $H_k^{\text{hot}}(t)$ in Eq. (2). Because of linearity, the mixing layer thickness $H_k^{\text{hot}}(t) - H_k^{\text{cold}}(t)$ and the interface location (the location of the isoline $F = 0.5$) can also be used to determine the F function. Because the location of the interface is the same for both velocity and temperature, considering the other parameters (the mixing layer thickness) are also identical for velocity and temperature, the same F can be used to describe velocity and temperature.

Because the thickness of the mixing layer is known, only one interface needs to be tracked, similar to what is done in a two-layer model. However, in contrast to two-layer models, the interface tracked in the three-layer model is the isoline for $F = 0.5$. Thus, the two interfaces between the three layers are determined by the thickness of thermal and flow boundary layers according to Eq. (4).

D. Equivalent Properties

To compute mass and energy transport and track the interfaces to account for the mixing layer effect, the equivalent properties in the upper and lower layers must be obtained by averaging each layer. In the three-layer model, equivalent properties can be estimated from

$$\bar{\phi}_L = \frac{1}{H_{\text{int}} - H_{\text{bot}}} \int_{H_{\text{bot}}}^{H_{\text{int}}} \phi(z)\mathrm{d}z \qquad \bar{\phi}_U = \frac{1}{H_{\text{top}} - H_{\text{int}}} \int_{H_{\text{int}}}^{H_{\text{top}}} \phi(z)\mathrm{d}z \tag{6}$$

where H_{int} denotes the height of the isoline for $F = 0.5$.

Assuming that the physical properties are uniform in the lower and upper layers, and substituting Eqs. (1) and (2) or (3–6), we obtain

$$\bar{\phi}_L = \frac{H_{\text{cold}} - H_{\text{bot}}}{H_{\text{int}} - H_{\text{bot}}}\phi_L + \frac{1}{H_{\text{int}} - H_{\text{bot}}} \int_{H_{\text{cold}}}^{H_{\text{int}}} [\phi_U F + \phi_L(1-F)]\mathrm{d}z \tag{7}$$

$$\bar{\phi}_U = \frac{H_{\text{top}} - H_{\text{hot}}}{H_{\text{top}} - H_{\text{int}}}\phi_U + \frac{1}{H_{\text{top}} - H_{\text{int}}} \int_{H_{\text{int}}}^{H_{\text{hot}}} [\phi_U F + \phi_L(1-F)]\mathrm{d}z \tag{8}$$

where $H_{\text{int}} = V_L/A$, $H_{\text{hot}} = V_L/A + \sqrt{\alpha_t t}$, and $H_{\text{cold}} = V_L/A - \sqrt{\alpha_t t}$.

E. Governing Equations

The governing equations of the three-layer model will be changed (from that for the two-layer model) due to mixing effects. First, from the ideal gas law and definitions of density and internal energy, subsidiary equations can be obtained as follows:

$$\bar{\rho}_L = P/R\bar{T}_L \qquad \bar{\rho}_U = P/R\bar{T}_U \tag{9}$$

$$\bar{M}_U = \bar{\rho}_U V_U \qquad \bar{M}_L = \bar{\rho}_L V_L \tag{10}$$

$$\bar{H}_U = C_v \bar{M}_U \bar{T}_U \qquad \bar{H}_L = C_v \bar{M}_L \bar{T}_L \tag{11}$$

$$V = V_L + V_U \tag{12}$$

where

$$\bar{T}_L = \frac{H_{\text{cold}} - H_{\text{bot}}}{H_{\text{int}} - H_{\text{bot}}} T_L + \frac{1}{H_{\text{int}} - H_{\text{bot}}} \int_{H_{\text{cold}}}^{H_{\text{int}}} [T_U F + T_L(1-F)]\mathrm{d}z$$

$$\bar{T}_U = \frac{H_{\text{top}} - H_{\text{hot}}}{H_{\text{top}} - H_{\text{int}}} T_U + \frac{1}{H_{\text{top}} - H_{\text{int}}} \int_{H_{\text{int}}}^{H_{\text{hot}}} [T_U F + T_L(1-F)]\mathrm{d}z$$

The additional governing equations are derived using the conservation of mass and energy, the ideal gas law, and the relations for density and internal energy.

$$\frac{\mathrm{d}P}{\mathrm{d}t} = \frac{\gamma - 1}{V}(\dot{\bar{H}}_L + \dot{\bar{H}}_U) \tag{13}$$

$$\frac{\mathrm{d}V_U}{\mathrm{d}t} = \frac{1}{\gamma P}\left[(\gamma - 1)\dot{\bar{H}}_U - V_U \frac{\mathrm{d}P}{\mathrm{d}t}\right] \tag{14}$$

$$\frac{\mathrm{d}T_U}{\mathrm{d}t} = \frac{1}{C_p \bar{\rho}_U V_U}\left(\dot{\bar{H}}_U - C_p \bar{T}_U \dot{\bar{M}}_U + V_U \frac{\mathrm{d}p}{\mathrm{d}t}\right) \tag{15}$$

$$\frac{\mathrm{d}T_L}{\mathrm{d}t} = \frac{1}{C_p \bar{\rho}_L V_L}\left(\dot{\bar{H}}_L - C_p \bar{T}_L \dot{\bar{M}}_L + V_L \frac{\mathrm{d}p}{\mathrm{d}t}\right) \tag{16}$$

From the above equations, it is evident that on the right hands of Eqs. (13–16) there exist integral averages $\bar{H}_L$, $\bar{H}_U$, $\bar{T}_U$, $\bar{T}_L$, $\bar{M}_U$, and $\bar{M}_L$ which are different from the two-layer model. From the formulas of $\bar{H}_L$, $\bar{H}_U$, $\bar{T}_U$, $\bar{T}_L$, $\bar{M}_U$, and $\bar{M}_L$, it is noted that the terms reflect the mass transport and heat exchange between the upper and the lower layers.

In addition, the mass of species such as carbon dioxide, carbon monoxide, soot, oxygen, etc., can be computed using the following transport equations:

$$\frac{\mathrm{d}m_s^U}{\mathrm{d}t} = \sum_{i=1}^{N} \dot{\bar{m}}_{s,i}^U \qquad s = 1, 2, \ldots, k \tag{17}$$

$$\frac{\mathrm{d}m_s^L}{\mathrm{d}t} = \sum_{i=1}^{N} \dot{\bar{m}}_{s,i}^L \qquad s = 1, 2, \ldots, k \tag{18}$$

where

$$\bar{m}_s^L = \frac{H_{\text{cold}} - H_{\text{bot}}}{H_{\text{int}} - H_{\text{bot}}} m_s^L + \frac{1}{H_{\text{int}} - H_{\text{cold}}} \int_{H_{\text{cold}}}^{H_{\text{int}}} [m_s^U F + m_s^L(1-F)]\mathrm{d}z \tag{19}$$

$$\bar{m}_s^U = \frac{H_{\text{top}} - H_{\text{hot}}}{H_{\text{top}} - H_{\text{int}}} m_s^U + \frac{1}{H_{\text{top}} - H_{\text{int}}} \int_{H_{\text{int}}}^{H_{\text{hot}}} [m_s^U F + m_s^L(1-F)]\mathrm{d}z \tag{20}$$

m_s^U and m_s^L denote the mass of the species s being tracked in the upper (U) and lower (L) layers, respectively.

From Eqs. (13–18), each formulation can be expressed in terms of rates of mass and enthalpy flow. These rates represent the exchange of mass and enthalpy between zones due to physical phenomena such as plumes, natural and forced ventilation, convective heat transfer, and radiation.

The mass and enthalpy source terms comprise the following modules:

$$\dot{\bar{M}}_U = \dot{\bar{M}}_{\text{HVENT}}^U + \dot{\bar{M}}_{\text{VVENT}}^U + \dot{\bar{M}}_{\text{MVENT}}^U + \dot{\bar{M}}_{\text{FIRE}}^U + \dot{\bar{M}}_{\text{DJFIRE}}^U \tag{21}$$

$$\dot{\bar{M}}_L = \dot{\bar{M}}^L_{\mathrm{HVENT}} + \dot{\bar{M}}^L_{\mathrm{VVENT}} + \dot{\bar{M}}^L_{\mathrm{MVENT}} + \dot{\bar{M}}^L_{\mathrm{FIRE}} + \dot{\bar{M}}^L_{\mathrm{DJFIRE}} \quad (22)$$

$$\dot{\bar{H}}_U = \dot{\bar{H}}^U_{\mathrm{HVENT}} + \dot{\bar{H}}^U_{\mathrm{VVENT}} + \dot{\bar{H}}^U_{\mathrm{MVENT}} + \dot{\bar{H}}^U_{\mathrm{FIRE}} + \dot{\bar{H}}^U_{\mathrm{DJFIRE}} + \dot{\bar{H}}^U_{\mathrm{CONV}} + \dot{\bar{H}}^U_{\mathrm{RAD}} + \dot{\bar{H}}^U_{\mathrm{CJ}} \quad (23)$$

$$\dot{\bar{H}}_L = \dot{\bar{H}}^L_{\mathrm{HVENT}} + \dot{\bar{H}}^L_{\mathrm{VVENT}} + \dot{\bar{H}}^L_{\mathrm{MVENT}} + \dot{\bar{H}}^L_{\mathrm{FIRE}} + \dot{\bar{H}}^L_{\mathrm{DJFIRE}} + \dot{\bar{H}}^L_{\mathrm{CONV}} + \dot{\bar{H}}^L_{\mathrm{RAD}} + \dot{\bar{H}}^L_{\mathrm{CJ}} \quad (24)$$

The terms on the right hands of the above equations are similar to the two-layer model CFAST, but all the terms use integral average properties such as $\bar{T}_U$, $\bar{T}_L$, $\bar{\rho}_U$, $\bar{\rho}_L$, etc. $\dot{\bar{M}}_{\mathrm{HVENT}}$, $\dot{\bar{M}}_{\mathrm{VVENT}}$, $\dot{\bar{M}}_{\mathrm{MVENT}}$, $\dot{\bar{M}}_{\mathrm{FIRE}}$, and $\dot{\bar{M}}_{\mathrm{DJFIRE}}$ denoting the mass exchange through the horizontal vents, the vertical vents, the mechanical ventilation system, the fires, and the door jet fires, respectively. $\dot{\bar{H}}_{\mathrm{HVENT}}$, $\dot{\bar{H}}_{\mathrm{VVENT}}$, $\dot{\bar{H}}_{\mathrm{MVENT}}$, $\dot{\bar{H}}_{\mathrm{FIRE}}$, $\dot{\bar{H}}_{\mathrm{DJFIRE}}$, $\dot{\bar{H}}_{\mathrm{CONV}}$, $\dot{\bar{H}}_{\mathrm{RAD}}$, and $\dot{\bar{H}}_{\mathrm{CJ}}$ denote the enthalpy exchange through the horizontal vents, the vertical vents, the mechanical ventilation system, the fires, the door jet fires, the convective heat transfer, the radiation, and the ceiling jet, respectively.

III. Results and Discussion

In this section, experimental data and CFD simulation-generated data will be used to compare the predictions from the three-layer model and that from the two-layer model.

A. Test 1: Validation with Experimental Data from Multiroom Fire

Cooper et al. conducted a series of experimental studies of multiroom fires [36]. Experimental data from this study are used for comparing the three-layer model and CFAST model predictions. The experiments involve two or three compartments, a fire source room, a corridor, and a lobby. There is a 2.0 m high and 1.07 m wide door between the fire source room and the corridor, and a 2.01 m high and 1.32 m wide door connecting the corridor and the lobby. In addition, there is a 0.15×0.94 m^2 hole in a wall surface of the corridor to the outside. The multiroom configuration for this study is shown in Fig. 3. The dimensions of the three compartments are listed in Table 1. The heat release rate is chosen to be a linearly growing fire with the relation $Q = Ct$, and $C = 0.5$ kW/s. The fuel properties and the fire location are listed in Table 2.

Two test cases are used. The first is a two-compartment test involving the fire source room and the corridor; the second is a three-compartment test involving the fire source room, the corridor, and the lobby. A, B, C, D, and E denote the location of instruments, including vertical arrays of eight thermocouples at each location that were used to measure the temperature profiles in [36]. A single pair of static pressure taps is located at A and C and located 0.05 m from the ceiling to measure pressure difference between the fire source room and the corridor [36].

Figure 4 presents the smoke layer interface height predicted by the three-layer model. In the three-layer model, the smoke layer interface

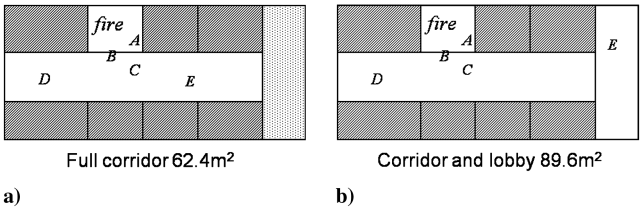

Fig. 3 Configuration of test 1 showing the instrument and fire location: a) case 1; b) case 2.

Table 1 Dimensions of the building in test 1

Compartments	Width, m	Depth, m	Height, m
Fire source room	4.3	3.3	2.36
Corridor	15.6	3.1	2.36
Lobby	3.0	9.0	2.36

Table 2 The fire properties used in test 1 simulation

Fuel	Methane (CH_4)
Heat of combustion, J/kg	5.0E + 7
Fire type	Confined
Location (width)	1.65
Location (depth)	2.15
Location (height)	0.24

is defined as the location of the isoline for $F = 0.5$. The three-layer model provides good predictions, as evident from the comparisons plotted.

Cooper et al. [36] defined and estimated the average temperature rise to be

$$\overline{\Delta T} = \frac{1}{H}\int_0^H [T(z,t) - T_{\mathrm{amb}}(z)]\mathrm{d}z \approx \frac{1}{H}\sum_n [T(z_n,t) - T_{\mathrm{amb}}(z_n)]\Delta z_n \quad (25)$$

Figure 5 displays the temporal variation of average temperature rise predicted by the three-layer model and experimental data in two indoor locations. The two-layer zone model CFAST is also used for comparison. Overall trends in the data are consistent with predictions from the two models. However, differences in some details are evident and insightful. Compared with the two-layer model CFAST, the three-layer model predicts a lower average temperature rise, which is closer to the experimental data, especially in the later stage of the fire development, where mixing is important. When hot gas enters the corridor through the vent, a mixing layer will form and diffuse (generally in the downward direction). In the early stages of the fire development process (i.e., when t is small), both the hot layer and the mixing layer ($\delta \propto \sqrt{t}$) are so thin that the mixing process has a minor effect on the mass and heat transfer. Thus, the difference between CFAST and the three-layer model is small. As time progresses, the upper layer becomes thicker, and the mass mixing and heat exchange in the mixing layer play a more important role in the temperature distribution. Although average temperature rise predictions from the three-layer model are qualitatively similar to those obtained by the two-layer model, the two-layer model overpredicts the temperature in the upper layer and underpredicts the temperature in the lower layer. These differences in the temperature profiles for the two-layer and the three-layer model predictions will be discussed later.

Experimental data (obtained from Cooper et al. [36]) for the time-varying, near-ceiling, pressure difference between the fire source room and the corridor can be compared to predictions by the present three-layer model and the CFAST model (see Fig. 6). The three-layer model reproduces the trend in the experimental data and the predictions are better than from CFAST, especially in the later stage of fire development, when mixing is important.

Although the agreement between the predictions of the three-layer model and those of experimental data are generally good, one notices that the pressure prediction of three-layer model becomes worse as time advances in Fig. 6. Generally, in the fire source room, the heat released in the fire results in a strong vertical flow of fire plume. This affects the smoke stratification in the fire room. Therefore the zone models may result in inaccurate predictions in such rooms. In the three-layer model, a piecewise linear F function is used to considered the mixing effects in regions of fire/smoke spread; however, mixing may not be the dominant physics in the fire source location.

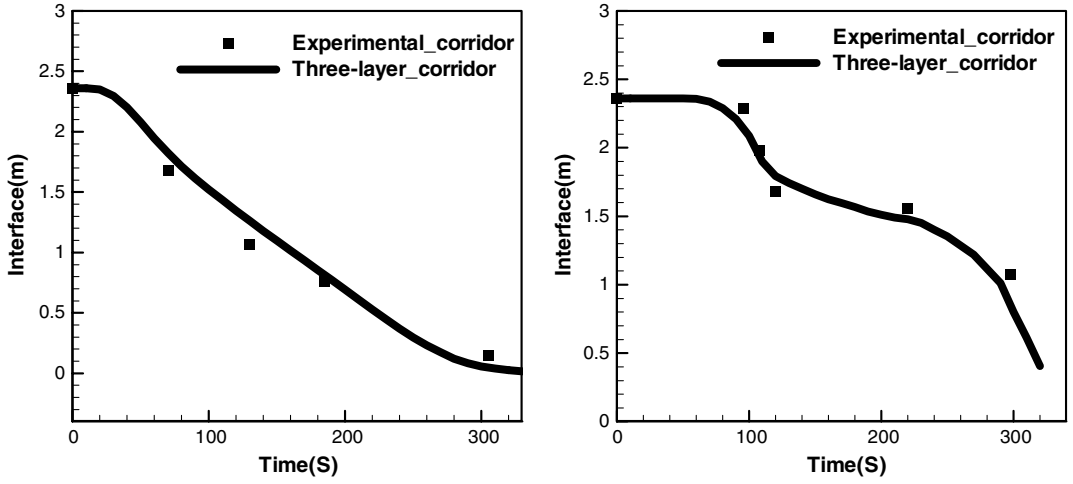

Fig. 4 Comparison of temporal variation of interface height using the three-layer model and experimental data: a) case 1; b) case 2.

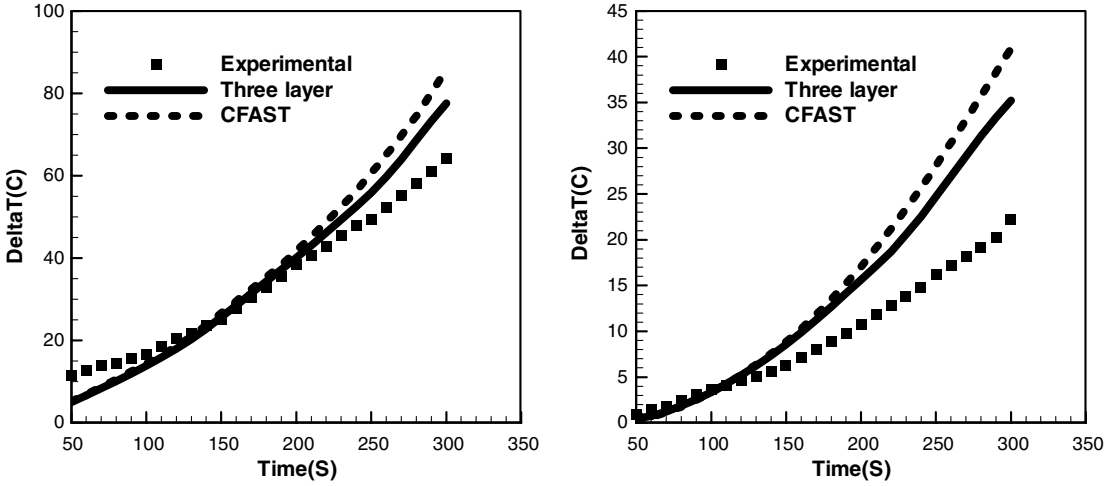

Fig. 5 Comparison of temporal variation of average temperature rise using the three-layer model, CFAST, and experimental data: a) the fire source room; b) the corridor.

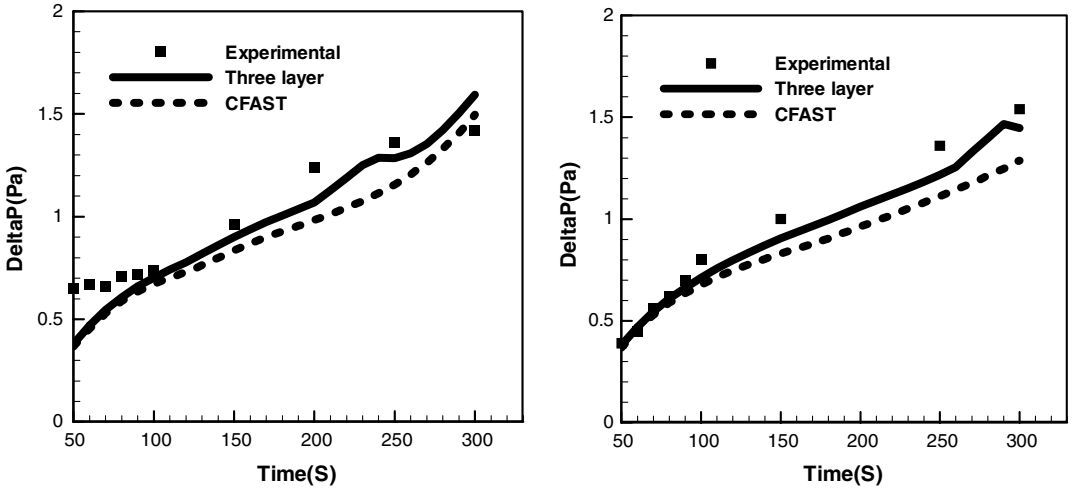

Fig. 6 Comparison of temporal variation of pressure difference between the fire source room and the corridor near the ceiling using the three-layer model, CFAST, and experimental data: a) case 1; b) case 2.

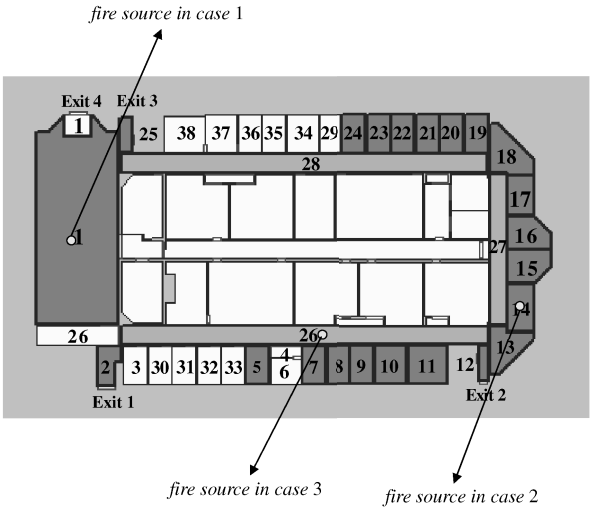

Fig. 7 The diagram of the building in test 2.

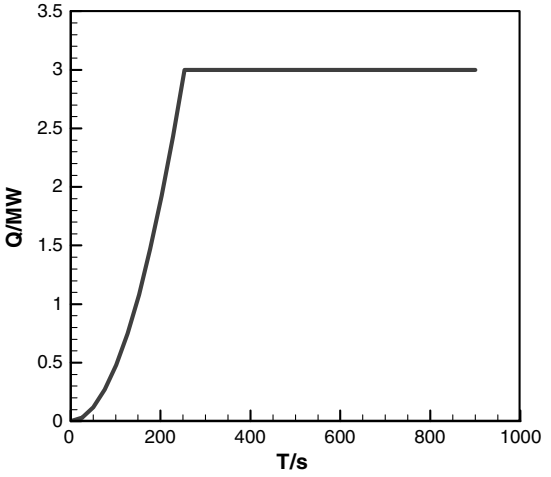

Fig. 8 Temporal variation of the heat release rate in test 2.

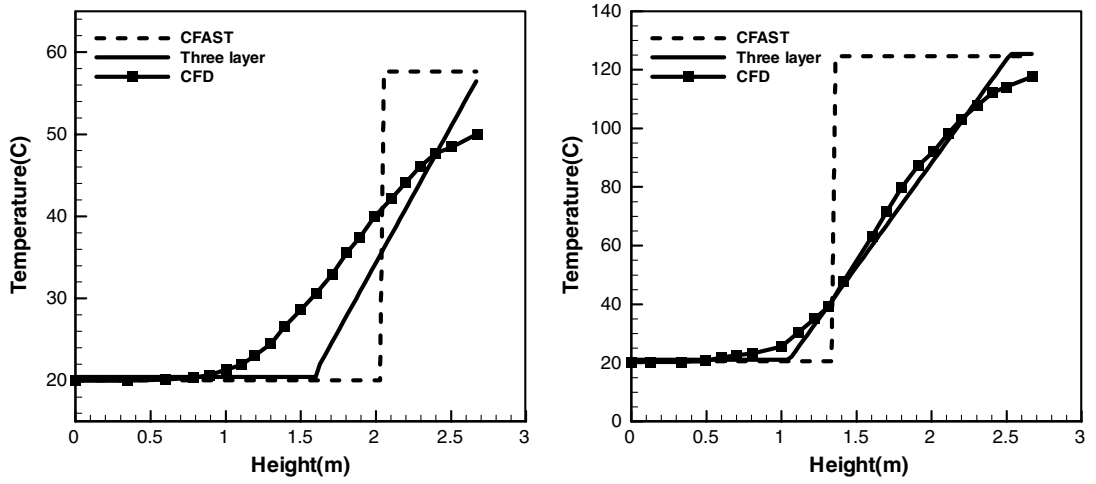

a) 150s b) 300s

Fig. 9 Temperature distributions in corridor 28 predicted using the three-layer model, CFAST, and CFD in case 1.

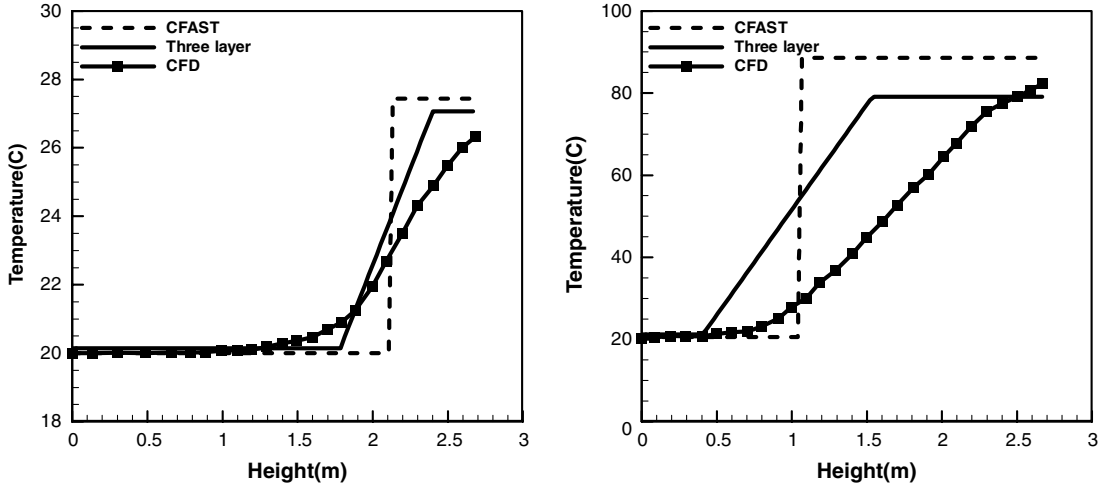

a) 150s b) 300s

Fig. 10 The temperature distributions in room 15 predicted using the three-layer model, CFAST, and CFD in case 2.

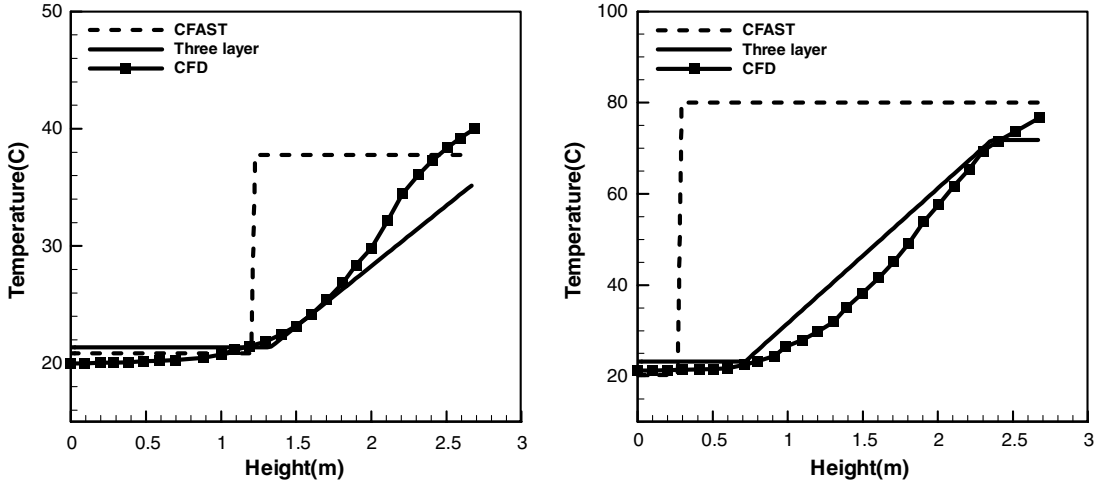

Fig. 11 The temperature distributions in corridor 27 predicted using the three-layer model, CFAST, and CFD in case 3.

The three-layer model will be more applicable for the rooms without a fire source. Although some empirical formulas obtained from experiments are also used to estimate the fire plume size and smoke generation rate, there exists a discrepancy as time advances especially for the pressure predictions due to importance of the energy exchange in the pressure equation (13).

B. Test 2: Model Comparison with CFD for Complex Building

A more complex building with more compartments is now used to assess the three-layer model predictions. Figure 7 illustrates the lower floor map of a two-story office building in the United Technologies Research Center (East Hartford, Connecticut). There are 35 compartments and three corridors, two of which are connected

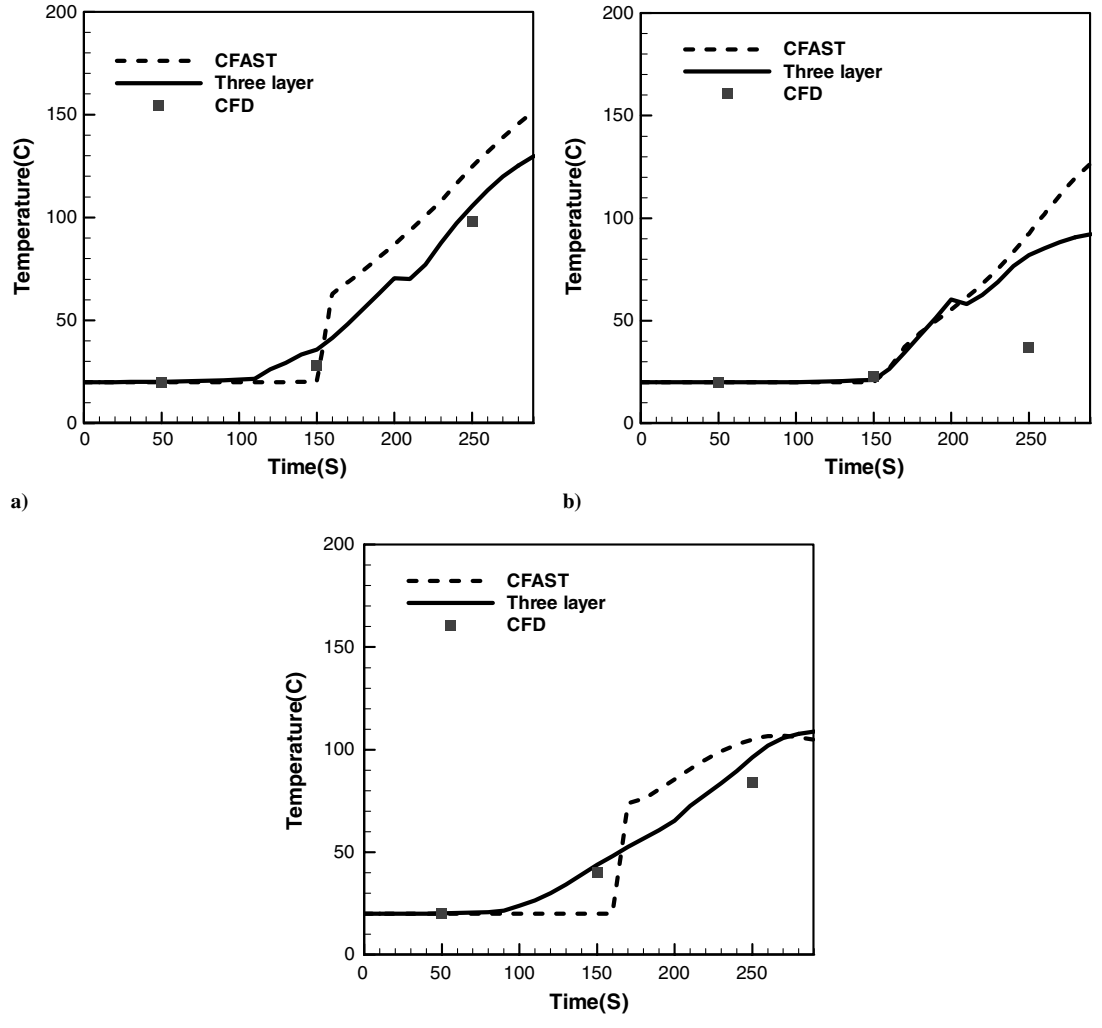

Fig. 12 Comparison of temporal variation of the temperature at the height of 2 m predicted using the three-layer model, CFAST, and CFD in case 1: a) corridor 26; b) corridor 27; and c) corridor 28.

to a lobby at the left side of the building. Twenty-five compartments in this building (rooms 1–25) are selected to be left open for the simulations here, allowing smoke to enter through doors connected by corridors. Corridor 26 has a height of 2.67 m, a width of 2.4 m, and a length of 59.7 m. Corridor 27 has a height of 2.67 m, a width of 2.0 m, and a length of 19.4 m. Corridor 28 has a height of 2.67 m, a width of 2.4 m, and a length of 49.0 m. The ventilation system is assumed to be turned off, as expected in the early moments of a fire event when fire and smoke detectors in the ventilation ducts trigger a shutdown.

Three fire scenarios are studied. In case 1, the fire source is located at the center of lobby 1. In case 2, the fire is started at the center of room 14. In case 3, the fire source is placed at the middle of corridor 26. In all three cases, the fire source is assumed to be located on the floor occupying a $1 \times 1 \times 1$ m^3 space. The three cases are simulated using the three-layer model, CFAST [8], and a CFD model (FLUENT [14]).

A heat source fire is used for this test. The heat release rate is chosen to be t^2 growing as $Q = 0.04689t^2$. The maximum heat release rate is 3 MW. The curve of the heat release rate is shown in Fig. 8.

In the CFD simulation, the fire source is treated as being of a volumetric heat generation type. The volume of the fire source is 1 m^3. The heat release rate Q is realized by using a user-defined function (UDF) which can be dynamically loaded with the FLUENT solver. The UDF q_v (W/m^3) is added as the source term to the energy equation. The relation between the heat release rate Q and the UDF q_v is $Q = V \cdot q_v$.

Figures 9–11 show the vertical temperature profiles at two time instants predicted by CFAST, the three-layer model, and the CFD model, for the three fire source cases. CFD predictions for the average temperature are displayed in three horizontal locations in the room: the center, one-fourth, and three-fourth widths of the room.

Predictions from the three-layer model are closer to those from FLUENT than those from CFAST. This shows that the proposed three-layer model can provide improved predictions of the vertical temperature profile, noting that the CFD model represents a more refined and accurate simulation. In CFAST, there is no mixing layer, so a sudden rise of the temperature at the interface and a higher maximum temperature is seen. The three-layer model predictions are closer to that from the CFD model, and the differences can be attributed to the thickness of the mixing layer. The thickness is affected by the turbulent eddy viscosity υ_t, which is a spatiotemporal variable and must be simulated using a turbulence model. In the current three-layer model, the turbulent viscosity is simply taken as a constant, thus not capturing the effect of turbulent diffusion accurately. This can lead to an uncertain prediction of the thickness of the mixing zone using the three-layer model.

Generally, physical properties, such as temperature at the height of 1.5–2.0 m, play an important role in evacuation, affecting the evacuation time and the behavior of occupants. From Figs. 9–11, this range (1.5–2.0 m) was found to be in the mixing layer or the lower layer. It would therefore be valuable for the model to consider the mixing effect between the hot and the cold layers. Figures 9–11 reveal that at the height of 1.5–2.0 m the new model indeed predicts a

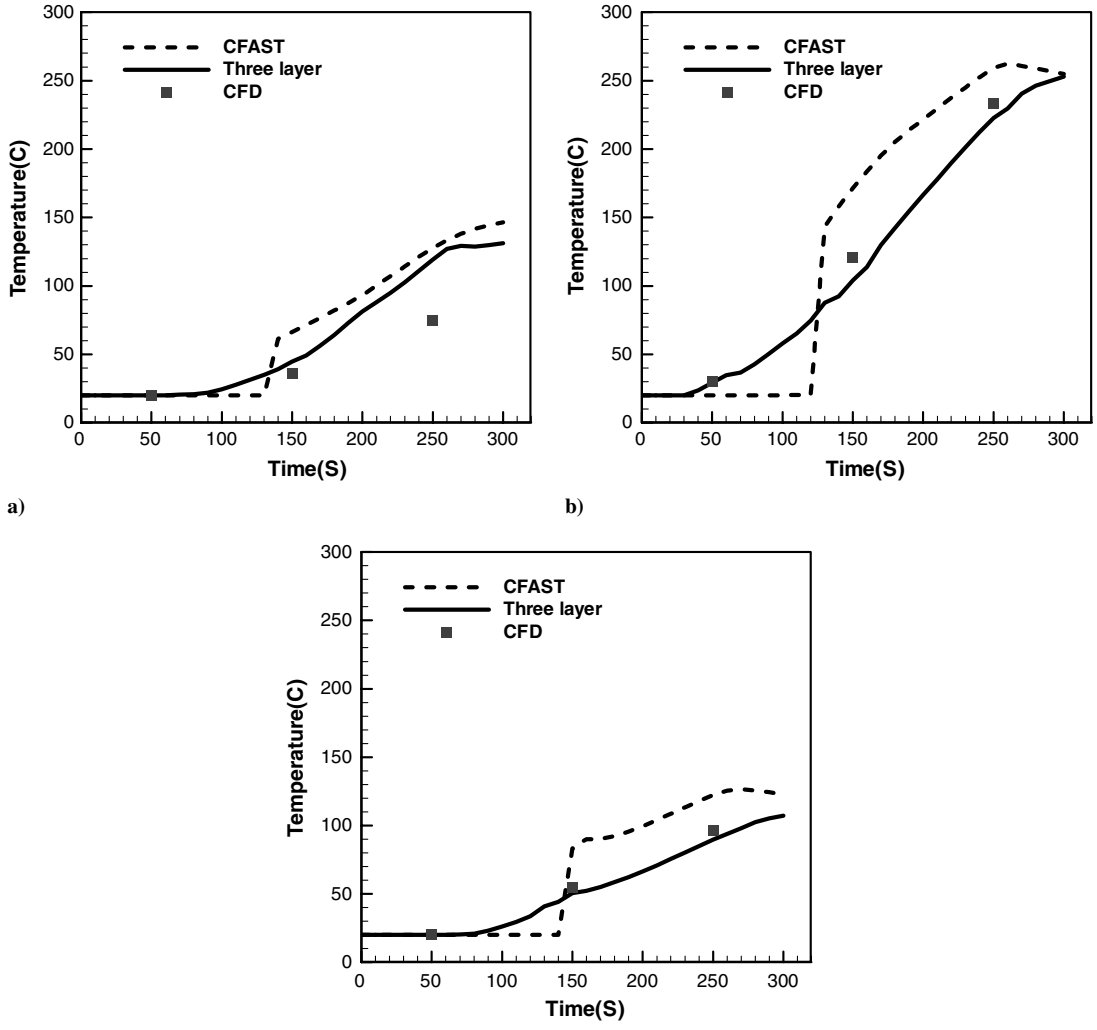

Fig. 13 Comparison of temporal variation of the temperature at the height of 2 m predicted using the three-layer model, CFAST, and CFD in case 2: a) corridor 26; b) corridor 27; and c) corridor 28.

temperature profile that is closer to that predicted by the CFD when compared to similar predictions by CFAST.

Observing the temperature distributions simulated in the three cases, the predictions in corridors as time advances (Fig. 9 and 11) are improved, whereas the agreement becomes worse in common compartments near the fire source (Fig. 10). The discrepancy may have resulted from the different characteristics of the smoke propagation in corridors and offices. For example, in corridors the mixing layer development takes more time and the mixing effect is more significant. Thus, during the development stage of the mixing layer, which lasts longer in corridors (maybe more than 300 s in cases 1 and 3), the three-layer model predictions are improved. In offices, as in case 2, because the development stage of the mixing layer may be much less than 300 s, we speculate that the improvement (as those of cases 1 and 3) should be evident but at much shorter times (such as at 150 s in Fig. 10a) and then become progressively worse (e.g., around 300 s in Fig. 10b). Thus, the three-layer model is likely to be more applicable to corridors at longer times and offices at shorter times. It should be noted that while compared to CFD simulations the predictions of the three-layer model in some rooms do get worse as time advances, as a less computationally expensive model, the three-layer model still provides better temperature predictions than the traditional zone model CFAST in all three cases from Figs. 9–11.

The temperature at a certain height is important for estimating the effects of smoke on occupants during evacuation and determines the activation time of the detection device. Moreover, physical properties such as the temperature and smoke layer height in corridors affect other compartments. We therefore focus our attention on the predictions in the three corridors. Figures 12–14 present the temperature at the height of 2 m in the three corridors predicted by the three-layer model, the CFAST, and the CFD models. CFD results are based on a large number of spatial grid points in two horizontal directions x and y, whereas the zone models predict the physical properties only in the vertical direction within a compartment. Thus, instead of using the field data, an average of the CFD results from three vertical profiles located at one-fourth, one-half, and three-fourth widths of the room, respectively, are used as the representative temperature of the whole zone.

Figures 12–14 illustrate that in all three cases the temperature at the height of 2 m predicted by the three-layer model is closer to that from the CFD model, especially in the corridors near the fire source. For case 1 (Fig. 12), the fire is located at lobby 1. Because of mixing of hot smoke and cold air in the fire source room, the temperature of the smoke entering corridors 26 and 28 is lower than that predicted by CFAST, which brings the temperature at the height of 2 m predicted by the three-layer model closer to the CFD result (see Figs. 12a and 12c). When the smoke in the mixing layer of corridors 26 and 28 propagates into corridor 27 at about 250 s, the temperature in corridor 27 becomes lower than that predicted by CFAST. Figure 12b shows that compared with the CFD result in corridor 27, the temperature is overpredicted. This is because in the current (three-layer) model the diffusion effect is only considered in the vertical direction, whereas, in fact, horizontal propagation and mixing will become important when the momentum transfer is weaker (such as when smoke enters corridor 27). The discrepancies

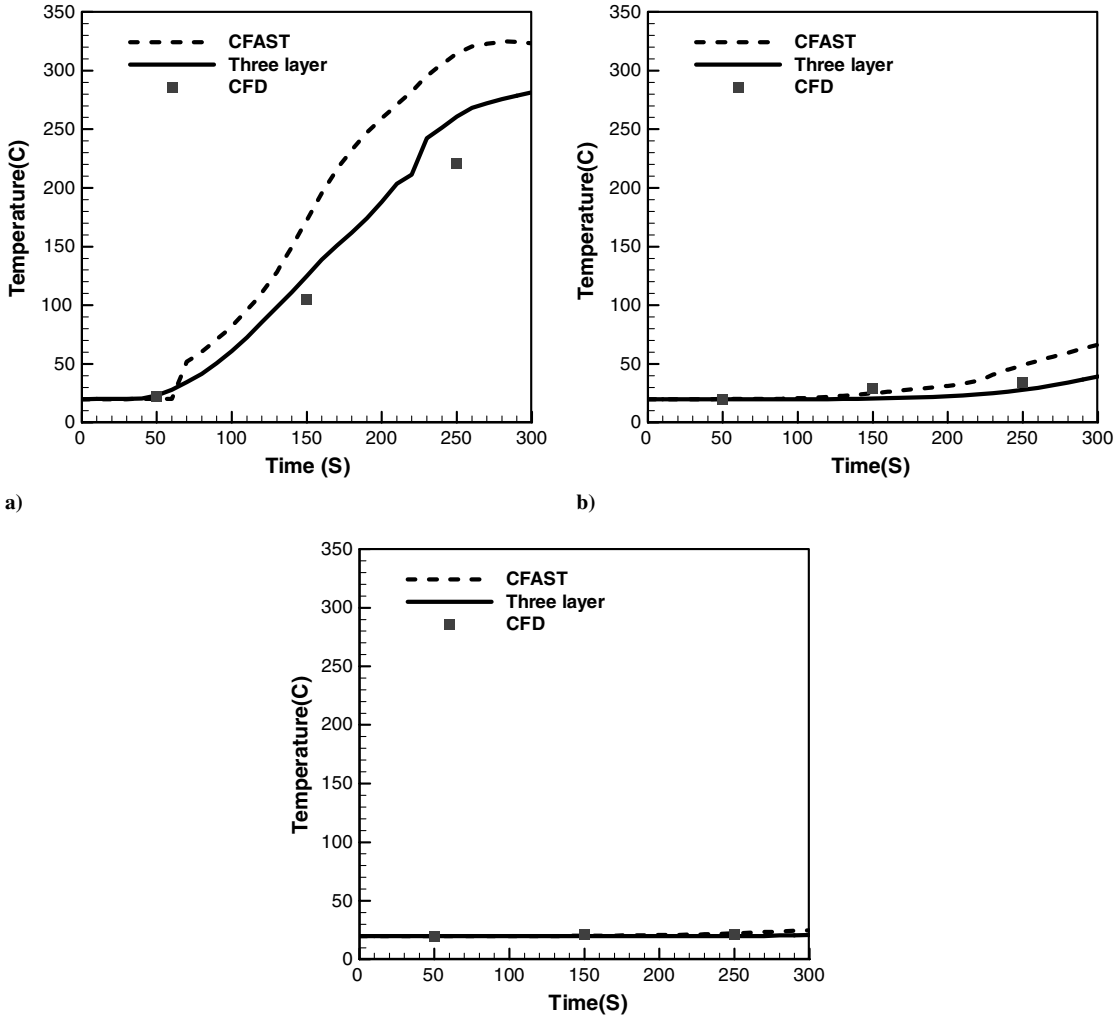

Fig. 14 Comparison of temporal variation of the temperature at the height of 2 m predicted using the three-layer model, CFAST, and CFD in case 3: a) corridor 26; b) corridor 27; and c) corridor 28.

between the three-layer model predictions and the CFD results become larger in the compartments farther away from the fire source.

The aforementioned analysis can also be used to explain Figs. 13 and 14.

The CPU time required by various models (CFAST, the three-layer model, and FLUENT) is an important factor to consider. Intel Core 2 Duo 2.4G CPU is used to benchmark the computation time for the different approaches simulating 300 s in actual time. When CFAST is used, it takes 8.41, 8.40, and 7.17 s to complete the simulations for the three cases. For the three-layer model it takes 14.95, 14.90, and 11.88 s to complete the three cases. For FLUENT, it takes 39, 42, and 38 h for the three cases. This shows that both the three-layer model and CFAST provide considerable computing time savings. On the other hand, although compared to CFAST, the CPU time increases when using the three-layer model, the difference is relatively small (when compared to that for CFD) and is considered to be acceptable for engineering and design calculations.

IV. Conclusions

A new model considering the effects of mixing during smoke propagation has been proposed, developed, and assessed using experimental data and higher fidelity simulations. The model enables fire and smoke propagation simulations in complex building structures and spaces. In contrast to traditional two-layer zone models, considering the mass transport and heat exchange between the upper and lower layers, a piecewise linear scalar function F is defined to divide the space into three layers (a hot layer, a cold layer, and a mixing layer); the properties in each zone are expressed as functions of F.

Multicompartment fire experimental data [36] were used to assess the new model and compare simulation results with predictions from a two-layer zone model (namely, CFAST). A realistic multiroom building fire connected by multiple paths was also simulated. In this case, a spatiotemporally well-resolved CFD simulation was used to provide the detailed field predictions needed to assess the three-layer model. The model predictions of the smoke layer height and average temperature profiles compared favorably with the experimental data and the CFD simulations.

The three-layer model predictions were found to be closer to the experimental data and CFD predictions when compared to similar predictions made using CFAST. The two-layer model implemented in CFAST predicts the temperature at some vertical height (such as 2 m) with a sudden temperature rise. In the new model, the temperature rises smoothly. CFAST usually overpredicts the temperature in the upper layer and underpredicts the temperature in the lower layer. The newly proposed zone model predicts lower temperature in the upper layer and higher temperature in the lower layer compared to CFAST, resulting in better predictions overall of the temperature distributions.

For the three-layer model presented here, properties in each zone are functions of time and the vertical height. It is recognized that the verification and validation of this model is preliminary, and a more detailed analysis is necessary (e.g., using a range of fire scenarios, building geometries, and boundary conditions) to understand the sensitivity of the model parameters and for model improvement. Further improvements can be accomplished by setting up the governing equations for F and coupling it to the zone model. This will enable consideration of the horizontal mixing effect during smoke propagation and introduce dependence on horizontal distance for physical properties such as temperature, layer height, and concentration of species.

Acknowledgment

The authors are grateful to United Technologies Research Center (UTRC) for financial support of this research.

References

[1] Zukoski, E. E., "Development of a Stratified Ceiling Layer in the Early Stages of a Closed-Room Fire," *Fire and Materials*, Vol. 2, No. 2, 1978, pp. 54, 62. doi:10.1002/fam.810020203

[2] Cooper, L. Y., "A Mathematical Model for Estimating Available Safe Egress Time in Fires," *Fire and Materials*, Vol. 6, Nos. 3–4, 1982, pp. 135, 144. doi:10.1002/fam.810060307

[3] Babrauskas, V., "COMPF2: A Program for Calculating Post-Flashover Fire Temperatures," National Institute of Standards and Technology, Gaithersburg, MD, NBS TN991, 1979.

[4] Davis, W. D., and Cooper, L. Y., "A Computer Model for Estimating the Response of Sprinkler Links to Compartment Fires with Draft Curtains and Fusible Link-Actuated Ceiling Vents," *Fire Technology*, Vol. 27, No. 2, 1991, pp. 113, 127. doi:10.1007/BF01470863

[5] Tanaka, T., "A Model of Multiroom Fire Spread," National Institute of Standards and Technology, Gaithersburg, MD, NBSIR 83-2718, 1983.

[6] Jones, W. W., "A Multicompartment Model for the Spread of Fire, Smoke and Toxic Gases," *Fire Safety Journal*, Vol. 9, No. 1, 1985, pp. 55, 79. doi:10.1016/0379-7112(85)90030-X

[7] Forney, G. P., and Cooper, L. Y., "The Consolidated Compartment Fire Model (CCFM) Computer Code Application CCFM.VENTs. Part 2: Software Reference Guide," National Institute of Standards and Technology, Gaithersburg, MD, NBSIR 90-4343, 1990.

[8] Jones, W. W., and Forney, G. P., "A Programmer's Reference Manual for CFAST, the Unified Model of Fire Growth and Smoke Transport," National Institute of Standards and Technology, Gaithersburg, MD, TN 1283, 1990.

[9] McGrattan, K. B., "Fire Dynamics Simulator (Ver. 4): Technical Reference Guide," National Institute of Standards and Technology, Gaithersburg, MD, NIST SP 1018, 2006.

[10] Ludwig, J. C., "PHOENICS-VR Reference Guide," CHAM—Concentration, Heat and Momentum Ltd., London, Technical Report TR/326, 2006.

[11] Cox, G., and Kumar, S., "Field Modelling of Fire in Forced Ventilated Enclosures," *Combustion Science and Technology*, Vol. 52, Nos. 1–3, 1987, pp. 7, 23. doi:10.1080/00102208708952565

[12] Ewer, J., Jia, F., Grandison, A., Galea, E., and Patel, M., *SMARTFIRE V4.0 User Guide and Technical Manual*, Fire Safety Engineering Group, University of Greenwich, London, England, U.K., 2004.

[13] Chow, W. K., and Yin, R., "A New Model on Simulating Smoke Transport with Computational Fluid Dynamics," *Building and Environment*, Vol. 39, No. 6, 2004, pp. 611, 620. doi:10.1016/j.buildenv.2003.12.012

[14] *FLUENT 6.0 Users' Guide*, Fluent Inc., 2001.

[15] Xu, T., Wang, J., and Fan, W., "A New Method of Modeling of a Fire: Combination of Field Modeling and Zone Modeling," *Proceedings of the Symposium on Engineering Thermo-Physics*, Chinese Association of Engineering Thermo-Physics, Zhenjiang, Jiangsu, 1991 (in Chinese).

[16] Wang, J., and Fan, W., "Numerical Simulation of Fire Process of Multi-Rooms," *Journal of University of Science and Technology of China*, Vol. 26, No. 2, 1996, pp. 204, 209 (in Chinese).

[17] Fan, W., and Wang, X., "A New Numerical Calculation Method for Zone Modelling to Predict Smoke Movement in Building Fires," *Fire Safety Science, Proceedings of the Fifth International Symposium*, International Association of Fire Safety Science, Melbourne, Australia, 1997. pp. 487, 498.

[18] Yao, J., Fan, W., Kohyu, S., and Daisuke, K., "Verification and Application of Field-Zone-Network Model in Building Fire," *Fire Safety Journal*, Vol. 33, No. 1, 1999, pp. 35, 44. doi:10.1016/S0379-7112(99)00006-5

[19] Yang, R., Jiang, Y., Ji, J., and Fan, W., "Development and Application of a Hybrid Field and Zone Numerical Model Based on Large Eddy Simulation in Buildings," *Progress in Natural Science*, Vol. 13, No. 6, 2003, pp. 637, 641 (in Chinese).

[20] Hua, J., Wang, J., and Kumar, K., "Development of a Hybrid Field and Zone Model for Fire Smoke Propagation Simulation in Buildings," *Fire Safety Journal*, Vol. 40, No. 2, 2005, pp. 99, 119. doi:10.1016/j.firesaf.2004.09.005

[21] Friedman, R., "An International Survey of Computer Models for Fire and Smoke," *Journal of Fire Protection Engineering*, Vol. 4, No. 3, 1992, pp. 81, 92. doi:10.1177/104239159200400301

[22] Charters, D. A., Gray, W. A., and McIntosh, A. C., "A Computer Model to Assess Fire Hazards in Tunnels (FASIT)," *Fire Technology*, Vol. 30, No. 1, 1994, pp. 134, 154. doi:10.1007/BF01040993

[23] Suzuki, K., Harada, K., and Tanaka, T., "A Multi-Layer Zone Model for Predicting Fire Behavior in a Single Room," *Fire Safety Science, Proceedings of the Seventh International Symposium*, International Association of Fire Safety Science, Worcester, MA, 2002.

[24] Zukoski, E. E., Kubota, T., and Lim, C. S., "Experimental Study of Environment and Heat Transfer in a Room Fire," National Institute of Standards and Technology, Gaithersburg, MD, NBS-GCR 85-493, 1985.

[25] Lim, C. S., Zukoski, E. E., and Kubota, T., "Mixing in Doorway Flows and Entrainment in Fire Plumes," National Institute of Standards and Technology, Gaithersburg, MD, NBS GCR 85-493, 1984.

[26] Steckler, K. D., Quintiere, J. G., and Rinkinen, W. J., "Flow Induced by Fire in a Compartment," National Institute of Standards and Technology, Gaithersburg, MD, NBSIR 82-2520, 1982.

[27] Wilcox, D. C., *Turbulence Modeling for CFD*, DCW Industries, La Canada, CA, 1994.

[28] Pope, S. B., *Turbulent Flows*, Cambridge Univ. Press, Cambridge, England, U.K., 2000.

[29] Rogers, M. M., and Moser, R. D., "Direct Simulation of a Self-Similar Turbulent Mixing Layer," *Physics of Fluids*, Vol. 6, No. 2, 1994, pp. 903, 923. doi:10.1063/1.868325.

[30] Bell, J. H., and Mehta, R. D., "Development of a Two-Stream Mixing Layer from Tripped and Untripped Boundary Layers," *AIAA Journal*, Vol. 28, No. 12, 1990, pp. 2034, 2042. doi:10.2514/3.10519

[31] Holman, J. P., *Heat Transfer*, McGraw–Hill, New York, 1990.

[32] Chow, W. K., and Li, J., "Numerical Simulations on Thermal Plumes with $k - \varepsilon$ Types of Turbulence Models," *Building and Environment*, Vol. 42, No. 8, 2007, pp. 2819, 2828. doi:10.1016/j.buildenv.2005.12.006

[33] Panchapakesan, N. R., and Lumley, J. L., "Turbulent Measurements in Axisymmetric Jets of Air and Helium," *Journal of Fluid Mechanics*, Vol. 246, No. 1, 1993, pp. 197–223. doi:10.1017/S0022112093000096

[34] Hussein, H. J., Capp, S., and George, W. K., "Velocity Measurements in a High-Reynolds-Number, Momentum-Conserving, Axisymmetric, Turbulent Jet," *Journal of Fluid Mechanics*, Vol. 258, No. 1, 1994, pp. 31–75. doi:10.1017/S002211209400323X.

[35] Fang, S. G., and Wu, B. S., "Study on the Value of Prandtl Number in Turbulent Buoyant Jet," *Journal of Basic Science and Engineering*, Vol. 14, No. 3, 2006, pp. 435, 443 (in Chinese).

[36] Cooper, L. Y., Harkleroad, M., Quintiere, J., and Rinkinen, W., "An Experimental Study of Upper Hot Layer Stratification in Full-Scale Multi-Room Fire Scenarios," *20th Joint ASME/AIChE National Heat Transfer Conference*, ASME 81-HT-9, American Society of Mechanical Engineers, New York, 1981.